*fractal and fractional*

MDPI

*Article*

# Efficient Analysis of Large-Size Bio-Signals Based on Orthogonal Generalized Laguerre Moments of Fractional Orders and Schwarz–Rutishauser Algorithm

**Eman Abdullah Aldakheel [1], Doaa Sami Khafaga [1], Islam S. Fathi [2], Khalid M. Hosny [3,*] and Gaber Hassan [4]**

[1] Department of Computer Sciences, College of Computer and Information Sciences, Princess Nourah bint Abdulrahman University, P.O. Box 84428, Riyadh 11671, Saudi Arabia; eaaldakheel@pnu.edu.sa (E.A.A.); dskhafga@pnu.edu.sa (D.S.K.)
[2] Department of Information Systems, Al Alson Higher Institute, Cairo 11762, Egypt; i_said76@yahoo.com
[3] Department of Information Technology, Faculty of Computers and Informatics, Zagazig University, Zagazig 44519, Egypt
[4] Department of Computer Science, Obour High Institute for Management & Informatics, Obour 11848, Egypt; gh_mcs86@yahoo.com
* Correspondence: k_hosny@yahoo.com or k_hosny@zu.edu.eg

**Abstract:** Orthogonal generalized Laguerre moments of fractional orders (FrGLMs) are signal and image descriptors. The utilization of the FrGLMs in the analysis of big-size signals encounters three challenges. First, calculating the high-order moments is a time-consuming process. Second, accumulating numerical errors leads to numerical instability and degrades the reconstructed signals' quality. Third, the QR decomposition technique is needed to preserve the orthogonality of the higher-order moments. In this paper, the authors derived a new recurrence formula for calculating the FrGLMs, significantly reducing the computational CPU times. We used the Schwarz–Rutishauser algorithm as an alternative to the QR decomposition technique. The proposed method for computing FrGLMs for big-size signals is accurate, simple, and fast. The proposed algorithm has been tested using the MIT-BIH arrhythmia benchmark dataset. The results show the proposed method's superiority over existing methods in terms of processing time and reconstruction capability. Concerning the reconstructed capability, it has achieved superiority with average values of 25.3233 and 15.6507 with the two metrics PSNR and MSE, respectively. Concerning the elapsed reconstruction time, it also achieved high superiority with an efficiency gain of 0.8. The proposed method is suitable for utilization in the Internet of Healthcare Things.

**Keywords:** bio-medical signals; signal reconstruction; fractional Laguerre moments; Schwarz–Rutishauser; internet of healthcare things; EEG; ECG; EMG



**Citation:** Aldakheel, E.A.; Khafaga, D.S.; Fathi, I.S.; Hosny, K.M.; Hassan, G. Efficient Analysis of Large-Size Bio-Signals Based on Orthogonal Generalized Laguerre Moments of Fractional Orders and Schwarz–Rutishauser Algorithm. *Fractal Fract.* **2023**, *7*, 826. https://doi.org/10.3390/fractalfract7110826

Academic Editor: Andjelija Ž. Ilić

Received: 14 October 2023
Revised: 12 November 2023
Accepted: 14 November 2023
Published: 16 November 2023



## 1. Introduction

The study of moments as a mathematical tool for describing 1-D, 2-D, and 3-D objects has become the focus of attention of many researchers since the middle of the previous century. Mathematically, the moments represent the projection of the object function onto certain functions called basis functions. This projection results in some statistical quantities representing significant features of the object [1]. One important type of moment is the Orthogonal Moments (OMs) set, where the basis functions are orthogonal. According to the object's coordinate space type, OMs exist in Continuous Orthogonal Moments (COMs) and Discrete Orthogonal Moments (DOMs) moments.

The first set of DOMs was discrete Tchebichef moments, which were introduced in 2001 by Mukundan et al. [2]. Later, many sets of DOMs were introduced, such as Krawtchouk moments, Hahn moments, Dual Hahn moments, Charlier moments, and Racah moments [3–7]. The different sets of DOMs are widely used in many signal and image processing applications, such as image reconstruction [8], image retrieval [9,10],

image compression [11,12], image steganography [13], and image watermarking [14]. DOMs reveal high-efficiency concerns representing different bio-medical signals: ECG, EEG, and EMG. Hosny et al. [15] suggested an efficient Algorithm for the compression of different types of bio-medical signals based on discrete Tchebichef moments and the Artificial Bee Colony (ABC). Fathi et al. [16–18] introduced different algorithms based on different types of DOMs for the efficient energy compression of bio-medical signals: ECG and FPCG. Such algorithms reveal high superiority concerning remote healthcare monitoring systems. In Cardiovascular Diseases (CVDs), continuous patient monitoring is very important for better diagnosis; healthcare systems that use ECG signals need long-term monitoring. As such, the size of the ECG signal collected by sensors to use in heart diagnosis is large. Concerning large-size bio-signals, Daoui et al. [19,20] suggested different approaches for reconstructing and compressing such signals. The presented approaches are based on Tchebichef moments and Meixner moments, respectively.

The successful utilization of DOMs with 2-D objects (i.e., images) motivates researchers to use these DOMs with 1-D objects (i.e., signals). Many studies used the DOMs as a feature descriptor for signals such as signal reconstruction and compression [15–17,21] and signal watermarking [22,23]. Other sets of moments are called complex moments. It is used basically in solving eigenvalue problems and has been used in image reconstruction applications. In the image reconstruction application, a formulation is shown to obtain an estimated original image from the degraded image moments and the blur parameter [24,25]. Complex Moments (CMs) were initially proposed as a straightforward and uncomplicated approach to reconstruction images. Still, the kernel functions of CMs lack orthogonality, which complicates reconstructing an image from its CMs.

Previous studies show that orthogonal moments of fractional orders outperformed their corresponding integer orthogonal moments of integer orders [26,27]. Orthogonal Moments of fractional orders are used to analyze medical signals, especially those characterized by their large size [19,20,28,29]. Despite the superiority of fractional versions of DOMs in many applications, some common problems occur when deriving the polynomial values: first, numerical instability results from the large increase (i.e., fluctuation) of the basis function values that occurs while increasing the moments' order. Secondly, a high computational time is required when calculating the polynomial values with the classical form of the polynomial equation. Thirdly, there is the propagation and accumulation of numerical errors, especially at higher orders, with large signals. These drawbacks cause the loss of the polynomial's orthogonality.

To overcome the previous problems, researchers used the weighted form of the fractional Chebychev polynomials, resulting in more numerical stability during calculations of polynomial values. Also, to overcome the highly time-consuming problem, they used a recurrence formula based on a normalization factor. The third problem vanished using the most common QR decomposition algorithms: the Gram–Schmidt Method (GSM), Householder Method (HM), and Given Rotations Method (GRM) [18].

In the current study, we introduced an efficient algorithm for large-size bio-signal signal reconstruction and analysis. The importance of this proposed algorithm lies in its high ability to compress the electrocardiogram (ECG) biomedical signals and transmit them over long distances in a short time. Also, due to this compression, the IoHT can transmit the ECG signals through a small bandwidth; hence, there is low energy consumption. The proposed algorithm depends on the set fractional-order generalized Laguerre moments (FrGLMs) and the Schwarz–Rutishauser approach. Through the current study, we derived three three-term second-order recurrence formulas for the normalized form of the FrGLMs. An important term when computing the normalized form of FrGLMs is the squared norm $h_k^{(\propto,\lambda)}$. By using the simple recursive formula of the gamma function, we deduced a recursive formula for evaluating the squared norm $h_k^{(\propto,\lambda)}$. The derived three-term recurrence formula with the recursive formula of the squared norm $h_k^{(\propto,\lambda)}$ has great benefits in saving computation time.

The utilization of the Schwarz–Rutishauser algorithm [30,31] is another contribution of this study, where the Schwarz–Rutishauser algorithm is used to preserve the orthogonality property when analyzing the large-sized bio-signals using high-order moments. The researchers are accustomed to using classical QR decomposition methods: the Gram–Schmidt Method (GSM), Householder Method (HM), and Given Rotations Method (GRM), but the empirical experiments reveal that the use of these leads to a significant increase in signal processing time, which leads to a lack of efficiency in both IoHT devices and real-time applications with the use of Schwarz–Rutishauser, which is an adaptation of the classical Gram–Schmidt. The complexity of the Schwarz–Rutishauser algorithm is $(\boldsymbol{mn}^2)$, which is $(\boldsymbol{n})$-times less than the complexity of the classical QR decomposition methods: GSM, HM, and GRM, which motivated us to use it in the proposed algorithm, which obtains better results concerning complexity and numerical stability. Uwe et al. [32] proved the efficiency of the Schwarz–Rutishauser algorithm concerning real-time fetal ECG monitoring systems, and it helped in raising the efficiency of the proposed system in terms of improving the system performance and energy consumption rate. To confirm the robustness of the FrGLMs with Schwarz–Rutishauser, samples of ECG bio-medical signal are used. These samples have been obtained from a benchmark dataset called MIT-BIH arrhythmia. An empirical experiment was carried out with the ECG bio-medical signals and revealed high superiority.

The contributions of this study are:

- A three-term second-order recurrence formula for the normalized form of FrGLMs has been derived.
- A recursive formula for the squared norm $h_k^{(\propto,\lambda)}$ has been derived.
- A novel QR-decomposition approach called Schwarz–Rutishauser gives more numerical stability and less processing time than the classical approaches.

The rest of this paper is: Section 2 briefly reviews the FrGLMs. Section 3 presents the proposed computations of the fractional generalized Laguerre polynomial (FrGLP). In Section 4, we introduce the proposed Schwarz–Rutishauser. The proposed algorithm of the FrGLMs based on the three-term second-order recurrence formula of the normalized FrGLP and the Schwarz–Rutishauser is discussed in detail in Section 5. The results are figured out and discussed in Sections 6 and 7, Respectively. The conclusions of this study are presented in Section 8.

## 2. Fractional-Order Generalized Laguerre Orthogonal Moments

The one-dimensional (1D) fractional-order generalized Laguerre orthogonal moments. $\mathrm{F_r\hat{L}M_i}$ with the order, i can be defined by the fractional-order generalized Laguerre polynomials $\mathrm{F_r\tilde{L}_i^{(\propto,\lambda)}}$ as follows:

$$\mathrm{F_r\hat{L}M}_i = \sum_{x=0}^{N-1} \mathrm{F_r\tilde{L}_i^{(\propto,\lambda)}}\, s(x), \quad i = 0, 1, 2, \ldots, N-1. \tag{1}$$

where $s(x)$ is a $(1 \times N)$ signal.

From the inverse transformation of fractional Laguerre moments, the original signal S(x) is reconstructed as follows:

$$S(x) = \sum_{i=0}^{i_{max}} \mathrm{F_r\hat{L}M}_i \mathrm{F_r\tilde{L}_i^{(\propto,\lambda)}}, \quad x = 0, 1, 2, \ldots, N-1. \tag{2}$$

where $F_r\hat{\mathrm{L}}\mathrm{M_i}$ *and* $\tilde{F_r L}_\mathrm{i}^{(\propto,\lambda)}$ are the fractional-order Laguerre moments and polynomials, respectively.

## 3. Proposed Computation of Fractional Laguerre Orthogonal Polynomials

The fractional-order generalized Laguerre polynomials (FGLPs) can be generated rapidly according to the following three-term recurrence formula [31]:

$$F_rL_{i+1}^{(\propto,\lambda)}(x) = \frac{1}{i+1}\left[\left(2i+\propto+1-x^{\lambda}\right)F_rL_i^{(\propto,\lambda)}(x) - (i+\propto)F_rL_{i-1}^{(\propto,\lambda)}(x)\right], \quad i = 1,2,\ldots,N \tag{3}$$

with the two initial conditions:

$$F_rL_0^{(\propto,\lambda)}(x) = 1 \text{ and } F_rL_1^{(\propto,\lambda)}(x) = 1+\propto -x^{\lambda}.$$

Also, the analytical form of $F_rL_i^{(\propto,\lambda)}(x)$ of the fractional degree $i\lambda$ can be obtained as:

$$F_rL_i^{(\propto,\lambda)}(x) = \sum_{k=0}^{i}(-1)^k\frac{\Gamma(i+\propto+1)}{\Gamma(k+\propto+1)(i-k)!k!}x^{\lambda k}, \quad i = 0,1,\ldots$$

The orthogonality property for FGLPs is also satisfied according to the following:

$$\int_0^{\infty} F_rL_j^{(\propto,\lambda)}(x)F_rL_k^{(\propto,\lambda)}(x)w^{(\propto,\lambda)}(x)dx = h_k,$$

where $w^{(\propto,\lambda)}(x)$ is the weight function, defined as follows:

$$w^{(\propto,\lambda)}(x) = \lambda x^{(\propto+1)\lambda-1}e^{-x^{\lambda}},$$

Also, the squared norm $h_k$ is defined as follows:

$$h_k^{(\propto,\lambda)} = \begin{cases} \frac{\Gamma(i+\propto+1)}{k!} & j = k, \\ 0, & j \neq k. \end{cases} \tag{4}$$

The normalized form of fractional-order generalized Laguerre polynomials (FGLPs) can obtained in terms of the weight and squared norm functions as follows:

$$\overset{\sim}{F_rL_i}^{(\propto,\lambda)}(x) = \sqrt{\frac{w^{(\propto,\lambda)}(x)}{h_k}}F_rL_i^{(\propto,\lambda)}(x), \tag{5}$$

Figure 1a,b illustrate the values of polynomials for normalized fractional Laguerre and the values of polynomials for fractional Laguerre for N = 100 and n = 0, 1, 2, 3, 4, and 5.

$$\alpha = 1,\ \lambda = 1.1.$$

The three-term recurrence relation of the normalized FGLPs ($\overset{\sim}{F_rL_i}^{(\propto,\lambda)}(x)$) can be deduced as follows.

At first, the two initial conditions can be obtained as the follows.

From Equations (3) and (5), one can deduce the following:

$$\overset{\sim}{F_rL_0}^{(\propto,\lambda)}(x) = \sqrt{\frac{w^{(\propto,\lambda)}(x)}{h_0}}F_rL_0^{(\propto,\lambda)}(x) = \sqrt{\frac{w^{(\propto,\lambda)}(x)0!}{\Gamma(0+\propto+1)}}F_rL_0^{(\propto,\lambda)}(x) = \sqrt{\frac{w^{(\propto,\lambda)}(x)}{\Gamma(\propto+1)}}, \tag{6}$$

and

$$\overset{\sim}{F_rL_1}^{(\propto,\lambda)}(x) = \sqrt{\frac{w^{(\propto,\lambda)}(x)}{h_1}}F_rL_1^{(\propto,\lambda)}(x) = \sqrt{\frac{w^{(\propto,\lambda)}(x)1!}{\Gamma(1+\propto+1)}}F_rL_1^{(\propto,\lambda)}(x) = \left(1+\propto-x^{\lambda}\right)\sqrt{\frac{w^{(\propto,\lambda)}(x)}{\Gamma(\propto+2)}}. \tag{7}$$

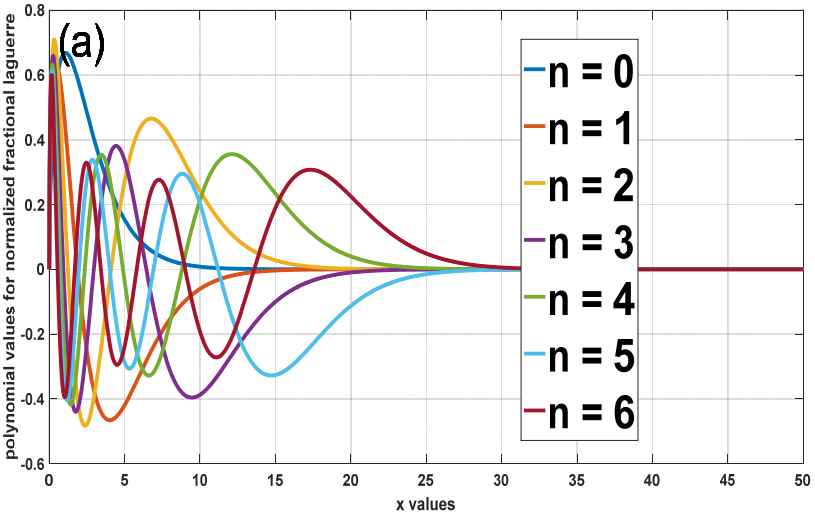


(**a**)

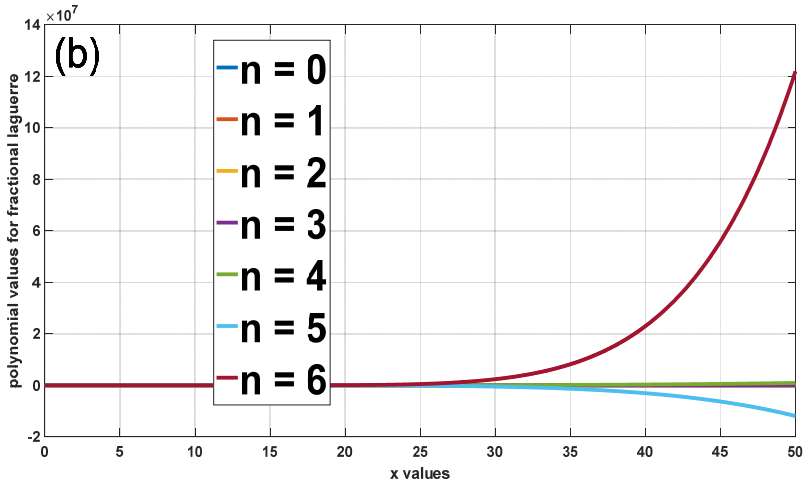


(**b**)

**Figure 1.** Plots of (**a**) $\tilde{F_r L_i}^{(\alpha,\lambda)}(x)$ and (**b**) $F_r L_{i+1}^{(\alpha,\lambda)}(x)$ for the first even orders with parameter values.

Secondly, the recurrence formula can be obtained as follows.

Based on the three-term recurrence relation of Equations (5) and (6), we can deduce the following:

$$\begin{aligned}\sqrt{\frac{h_{i+1}}{w^{(\alpha,\lambda)}(x)}}\tilde{F_r L}_{i+1}^{(\alpha,\lambda)}(x) &= \frac{1}{i+1}\left[(2i+\alpha+1-x^{\lambda})\sqrt{\frac{h_1}{w^{(\alpha,\lambda)}(x)}}\tilde{F_r L}_i^{(\alpha,\lambda)}(x) - (i+\alpha)\sqrt{\frac{h_{i-1}}{w^{(\alpha,\lambda)}(x)}}\tilde{F_r L}_{i-1}^{(\alpha,\lambda)}(x)\right], i = 1,2,\ldots\\ \sqrt{h_{i+1}}\tilde{F_r L}_{i+1}^{(\alpha,\lambda)}(x) &= \frac{1}{i+1}\left[(2i+\alpha+1-x^{\lambda})\sqrt{h_i}\tilde{F_r L}_i^{(\alpha,\lambda)}(x) - (i+\alpha)\sqrt{h_{i-1}}\tilde{F_r L}_{i-1}^{(\alpha,\lambda)}(x)\right].\end{aligned} \tag{8}$$

By using the recursive formula of the gamma function, one can deduce the following:

$$\Gamma(k+\alpha+1) = (k+\alpha)\Gamma(k+\alpha), \tag{9}$$

by substituting from Equation (9) into Equation (4):

$$\begin{aligned}h_k^{(\alpha,\lambda)} &= \frac{\Gamma(\alpha+k+1)}{k!} = \frac{(k+\alpha)\Gamma(k+\alpha)}{k(k-1)!} = \frac{(k+\alpha)}{k}\frac{\Gamma(k+\alpha)}{(k-1)!} = \frac{(k+\alpha)}{k}h_{k-1}^{(\alpha,\lambda)},\\ h_k^{(\alpha,\lambda)} &= \frac{(k+\alpha)}{k}h_{k-1}^{(\alpha,\lambda)}.\end{aligned} \tag{10}$$

Equation (10) represents a recursive formula for evaluating the squared norm $h_k^{(\propto,\lambda)}$. This formula has great benefits in saving computation time.

From Equation (10), we can deduce the following:

$$h_k^{(\propto,\lambda)} = \frac{(k+\propto)}{k} h_{k-1}^{(\propto,\lambda)} = \frac{(k+\propto)}{k} \frac{(k+\propto-1)}{k-1} h_{k-2}^{(\propto,\lambda)}, \tag{11}$$

$$h_{k+1}^{(\propto,\lambda)} = \frac{(k+\propto+1)}{k+1} h_k^{(\propto,\lambda)} = \frac{(k+\propto+1)}{k+1} \frac{(k+\propto)}{k} \frac{(k+\propto-1)}{k-1} h_{k-2}^{(\propto,\lambda)}, \tag{12}$$

$$h_{k-1}^{(\propto,\lambda)} = \frac{(k+\propto-1)}{k-1} h_{k-2}^{(\propto,\lambda)}. \tag{13}$$

Equation (8) can be rewritten as follows:

$$\overset{\sim}{F_r L}_{i+1}^{(\propto,\lambda)}(x) = \frac{1}{i+1}\left[\left(2i+\propto+1-x^{\lambda}\right)\frac{\sqrt{h_i}}{\sqrt{h_{i+1}}}\overset{\sim}{F_r L}_i^{(\propto,\lambda)}(x) - (i+\propto)\frac{\sqrt{h_{i-1}}}{\sqrt{h_{i+1}}}\overset{\sim}{F_r L}_{i-1}^{(\propto,\lambda)}(x)\right], \tag{14}$$

from Equations (11)–(13):

$$\frac{\sqrt{h_k}}{\sqrt{h_{k+1}}} = \sqrt{\frac{(k+1)}{(\propto+k+1)}}, \tag{15}$$

$$\frac{\sqrt{h_{k-1}}}{\sqrt{h_{k+1}}} = \sqrt{\frac{k(k+1)}{(\propto+k+1)(\propto+k)}}. \tag{16}$$

By substituting from Equations (15) and (16) into Equation (14):

$$\overset{\sim}{F_r L}_{i+1}^{(\propto,\lambda)}(x) = \frac{\left(2i+\propto+1-x^{\lambda}\right)}{(i+1)}\sqrt{\frac{(i+1)}{(\propto+i+1)}}\overset{\sim}{F_r L}_i^{(\propto,\lambda)}(x) - \frac{(i+\propto)}{(i+1)}\sqrt{\frac{i(i+1)}{(\propto+i+1)(\propto+i)}}\overset{\sim}{F_r L}_{i-1}^{(\propto,\lambda)}(x), \tag{17}$$

## 4. Schwarz–Rutishauser Algorithm

The Schwarz–Rutishauser algorithm adapts the classical Gram–Schmidt methods [30,33–35]. The Gram–Schmidt is a decomposition of matrix A as:

$$A = QR \tag{18}$$

where $Q$ is an orthogonal matrix and $R$ is an upper triangular matrix. The orthogonal matrix $Q$ is produced based on the orthogonal projection. An orthogonal projection of $a$ onto $q$ is:

$$proj_{\vec{q}}\vec{a} = \frac{\left\langle \vec{q}, \vec{a} \right\rangle}{\left\langle \vec{q}, \vec{q} \right\rangle} \times \vec{q} = \frac{\left\langle \vec{q}, \vec{a} \right\rangle}{\left\| \vec{q} \right\|^2} \times \vec{q} \tag{19}$$

Each orthogonal vector q ∈ Q is determined by calculating the sum of projections and subtracting it from the corresponding vector a ∈ A. The entire Gram–Schmidt process yields an orthogonal matrix $Q$ and can be expressed as:

$$\vec{q}_k = \vec{a}_k - \sum_{i=1}^{k-1} proj_{\vec{q}_i}\vec{a}_k, \tag{20}$$

$$\vec{q}_k = \frac{\vec{q}_k}{\left\| \vec{q}_k \right\|}. \tag{21}$$

The Gram–Schmidt method exhibits several drawbacks, including numerical instability and a significant increase in computational complexity for orthogonalizing matrices of a considerable size. The motivation behind the development of the Schwarz–Rutishauser

algorithm stemmed from the objective of minimizing the computational complexity associated with the prevailing Gram–Schmidt projection-based approaches and improving their numerical stability.

Equation (21) can be simplified by removing the division by the squared norm from the sum of projections as follows:

$$\vec{q}_k = \vec{a}_k - \sum_{i=1}^{k-1} \left\langle \vec{q}_i^{\,T}, \vec{a}_k \right\rangle \times \vec{q}_i \tag{22}$$

We can easily find the i-th element of each column vector r by using the formula:

$$\vec{e}_k r_{i,k} = \left\langle \vec{q}_i^{\,T}, \vec{a}_k \right\rangle \vec{e}_k \tag{23}$$

By substituting the Equation (23) in (22):

$$\vec{q}_k = \vec{a}_k - \sum_{i=1}^{k-1} r_{k-1,k} \times \vec{q}_{k-1} \tag{24}$$

Based on Equations (23) and (24) above, this can be done recursively:

$$r_{i,k} = \left\langle \vec{q}_i^{\,T}, \vec{q}_k \right\rangle \tag{25}$$

$$\vec{q}_k = \vec{a}_k - r_{k-1,k} \times \vec{q}_{k-1} \tag{26}$$

We subtract the product of the vector $q_i \in (k)$ and $r_i$ from the vector $q$, which is the vector rejection of $a$. That is why the sum operator can be removed from Equation (24).

Besides the $q$, we compute the $r$ $k$th diagonal element in $R$, as the norm $|q|$:

$$r_{k,k=} \left\| \vec{q}_k \right\| \tag{27}$$

## 5. Proposed Computation of Fractional Laguerre Orthogonal Moments Based on the Schwarz–Rutishauser Algorithm

Generally, the proposed signal analysis algorithm has two main methods: FrGLMs and Schwarz–Rutishauser. FrGLMs extract features from the signals and Schwarz–Rutishauser to preserve numerical stability with less complexity. The proposed algorithm is described as six steps. In step 1, set the maximum value (L) and ($L_{max}$) as the order of polynomials. Step 2 illustrates calculating the two initial conditions, $\overset{\sim}{F_r L_0}^{(\propto,\lambda)}(x)$ and $\overset{\sim}{F_r L_1}^{(\propto,\lambda)}(x)$, using the following equations:

$$\overset{\sim}{F_r L_0}^{(\propto,\lambda)}(x) = \sqrt{\frac{w^{(\propto,\lambda)}(x)}{\Gamma(\propto+1)}},$$
$$\overset{\sim}{F_r L_1}^{(\propto,\lambda)}(x) = (1+\propto -x^{\lambda}) \sqrt{\frac{w^{(\propto,\lambda)}(x)}{\Gamma(\propto+2)}}$$

In step 3, calculate the polynomials of order $i$ depending on the initial conditions by the below equation:

$$\overset{\sim}{F_r L_{i+1}}^{(\propto,\lambda)}(x) = \frac{(2i+\propto+1-x^{\lambda})}{(i+1)} \sqrt{\frac{(i+1)}{(\propto+i+1)}} \overset{\sim}{F_r L_i}^{(\propto,\lambda)}(x) - \frac{(i+\propto)}{(i+1)} \sqrt{\frac{i(i+1)}{(\propto+i+1)(\propto+i)}} \overset{\sim}{F_r L_{i-1}}^{(\propto,\lambda)}(x)$$

After computing Laguerre polynomials of orders i, in step 4, we use the Schwarz–Rutishauser to obtain the orthogonal matrix $Q$ and normalize $Q$ by dividing it by its norm using the following equations:

$$r_{n,m} = \left\langle \overrightarrow{Q}^{T}_{1:L,n}, \overrightarrow{Q}_{1:L,m} \right\rangle,$$
$$Q_{1:L,m} = Q_{1:L,m} - r_{n,m} \times Q_{1:L,n},$$
$$Q_{1:L,m} = Q_{1:L,m} / \|Q_{1:L,m}\|.$$

In step 5, the fractional-order generalized Laguerre moments are applied on matrix $Q$ to get the features from the signal using the following equation:

$$\mathrm{F_r\hat{L}M_i} = \sum_{\mathrm{x}=0}^{\mathrm{N}-1} \mathrm{F_rL_i}^{\sim(\propto,\lambda)} \mathrm{s(x)}, \quad \mathrm{i} = 0, 1, 2, \ldots, \mathrm{N}-1$$

Then, apply the inverse of the fractional Laguerre moments to get the reconstructed signal $\mathrm{S(x)}$ based on the below equation:

$$\mathrm{S(x)} = \sum_{\mathrm{i}=0}^{\mathrm{i_{max}}} \mathrm{F_r\hat{L}M_iF_r}\overset{\sim}{\mathrm{L}}_{\mathrm{i}}^{(\propto,\lambda)}, \quad \mathrm{x} = 0, 1, 2, \ldots, \mathrm{N}-1.$$

*An Algorithm of the Proposed Method*

The algorithm's pseudo code is presented in Algorithm 1.

**Algorithm 1. The algorithm's pseudo-code**

{—— Step 1: Determine the value L and $\mathbf{L_{max}}$——}
Input the original signal $\boldsymbol{s}(\boldsymbol{x})$
Set the highest value (L) of variable x.
Set a polynomial's order ($\boldsymbol{L_{max}}$).
{——Step 2: Calculate the initial conditions of the polynomials——}
for x←0 to L-1 do
Calculate $\overset{\sim}{\boldsymbol{F_rL_0}}^{(\propto,\lambda)}(\boldsymbol{x})$ using Equation (6).
Calculate $\overset{\sim}{\boldsymbol{F_rL_1}}^{(\propto,\lambda)}(\boldsymbol{x})$ using Equation (7).
{—— Step 3: Calculate the polynomials of order i ——}
for $\boldsymbol{i} \leftarrow \mathbf{2}$ to $\boldsymbol{L_{max}} - \mathbf{1}$ do
Calculate $\overset{\sim}{\boldsymbol{F_rL_i}}^{(\propto,\lambda)}(\boldsymbol{x})$ using Equation (17).
end for
{—— Step 4: Obtain the orthogonal matrix Q using the Schwarz-Rutishauser ——}
$\boldsymbol{FL} = \overset{\sim}{\boldsymbol{F_rL_i}}^{(\propto,\lambda)}(\boldsymbol{x})$
For n ← **1** to L do
$\boldsymbol{Q_{1:N,n}} = \boldsymbol{FL_{1:N,n}}$
for $\boldsymbol{m} \leftarrow \mathbf{0}$ to $\mathbf{n}-\mathbf{1}$ do
$\boldsymbol{r_{n,m}} = \left\langle \overrightarrow{\boldsymbol{Q}}^{T}_{\boldsymbol{1:L,n}}, \overrightarrow{\boldsymbol{Q}}_{\boldsymbol{1:L,m}} \right\rangle$
$\boldsymbol{Q_{1:L,m}} = \boldsymbol{Q_{1:L,m}} - \boldsymbol{r_{n,m}} \times \boldsymbol{Q_{1:L,n}}$
end for
$\boldsymbol{Q_{1:L,m}} = \boldsymbol{Q_{1:L,m}} / \|\boldsymbol{Q_{1:L,m}}\|$
end for
end for
{— —Step 5: Get the features of the input signal using Fractional Laguerre moments ——}
Apply fractional Laguerre moments ($\mathbf{F_r\hat{L}M}_{\boldsymbol{i}}$) using Equation (1).
{—— Step 6: return the reconstructed signal ——}
Apply the inverse of fractional Laguerre moments to get the reconstructed signal $\boldsymbol{S}(\boldsymbol{x})$ using Equation (2).

## 6. Experiments and Discussion

We utilized some ECG signals from the MIT-BIH Arrhythmia Dataset in the experiments. The Mean Squared Error (MSE) and Peak Signal-to-Noise Ratio (PSNR) are utilized to evaluate the efficacy of the introduced algorithm [36].

- **Relative error (RelErr (%))**

The relative error is calculated by dividing the absolute error of the measurement by the value of the measurement itself:

$$\text{RelErr} = \left( \frac{stdev(f(x) - F(x))}{|f(x)|} \right) \times 100\% \tag{28}$$

- **Mean Squared Error (MSE)**

The Mean Squared Error (MSE) measures the average of the squares of the errors, that is, the average squared difference between the reconstructed signal F(x) and the original signal f(x):

$$\text{MSE} = \frac{1}{\text{N}} \sum_{\text{x}=0}^{\text{N}-1} \left( \text{f(x)} - \text{F(x)} \right)^2 \tag{29}$$

- **Peak Signal-to-Noise Ratio (PSNR)**

PSNR is a metric that quantifies the relationship between the maximum achievable signal power and the power of the noise that distorts it:

$$\text{SNR} = 20 \times \log_{10} \frac{max|f(x)|}{\sqrt{MSE}} \tag{30}$$

where $f(x)$ is the original signal, and $F(x)$ is a reconstructed signal.

*Results*

In this section, an experimental examination of the proposed algorithm is carried out to investigate and assess its performance in reconstructing the signals utilizing various scenarios. Table 1 presents the proposed algorithm's and FrGLMs' comparative results on some signals from the MIT-BIH Arrhythmia Dataset. The results illustrate the superiority of the proposed algorithm in reconstruction metrics (PSNR = 143.21, MSE = 0.01096, and RelErr (%) = 0.027) over using FrGLMs; this can also be seen in Figure 2.

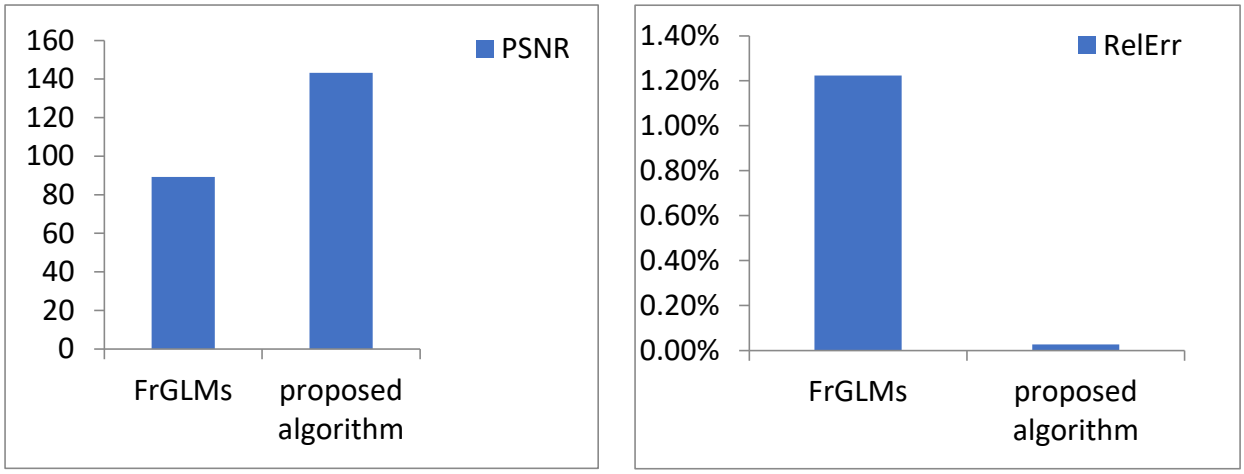


**Figure 2.** The average values of quality metrics (PSNR and RelErr (%)) for the introduced algorithm and FrGLMs.

**Table 1.** Empirical results of the introduced algorithm compared with FrGLMs.

| Signal | FrGLMs | | | Proposed Algorithm | | |
|---|---|---|---|---|---|---|
| | PSNR | MSE | RelErr (%) | PSNR | MSE | RelErr (%) |
| **Rec. 101** | 84.61 | 0.23005 | 0.57 | 141.05 | 0.00992 | 0.025 |
| **Rec. 108** | 70.06 | 0.967 | 2.398 | 119.92 | 0.01496 | 0.037 |
| **Rec. 115** | 110.88 | 0.037 | 0.092 | 155.46 | 0.00328 | 0.008 |
| **Rec. 209** | 66.65 | 0.83865 | 2.079 | 135.82 | 0.00728 | 0.018 |
| **Rec. 214** | 80.83 | 0.60155 | 1.492 | 139.8 | 0.0304 | 0.075 |
| **Rec. 219** | 112.49 | 0.05465 | 0.136 | 163.2 | 0.00808 | 0.02 |
| **Rec. 230** | 78.05 | 0.722 | 1.79 | 151.41 | 0.00456 | 0.011 |
| **Rec. 234** | 74.11 | 0.49475 | 1.227 | 139.05 | 0.00936 | 0.023 |
| **Average** | **89.21** | **0.4932** | **1.223** | **143.21** | **0.01096** | **0.027** |

Table 2 shows the numerical results of the proposed algorithm against the algorithms that use GSM, HM, and GRM. The results in Table 1 demonstrate the advantage of the proposed algorithm over the other methods (GSM, HM, and GRM). The proposed algorithm achieves the best PSNR (143.21), MSE (0.01096), and RelErr (0.027%). Figure 3 depicts the average PSNR and RelErr of the proposed algorithm and other signal reconstruction algorithms employing GSM, HM, and GRM. It demonstrates that the introduced algorithm is superior in the reconstructed signal quality.

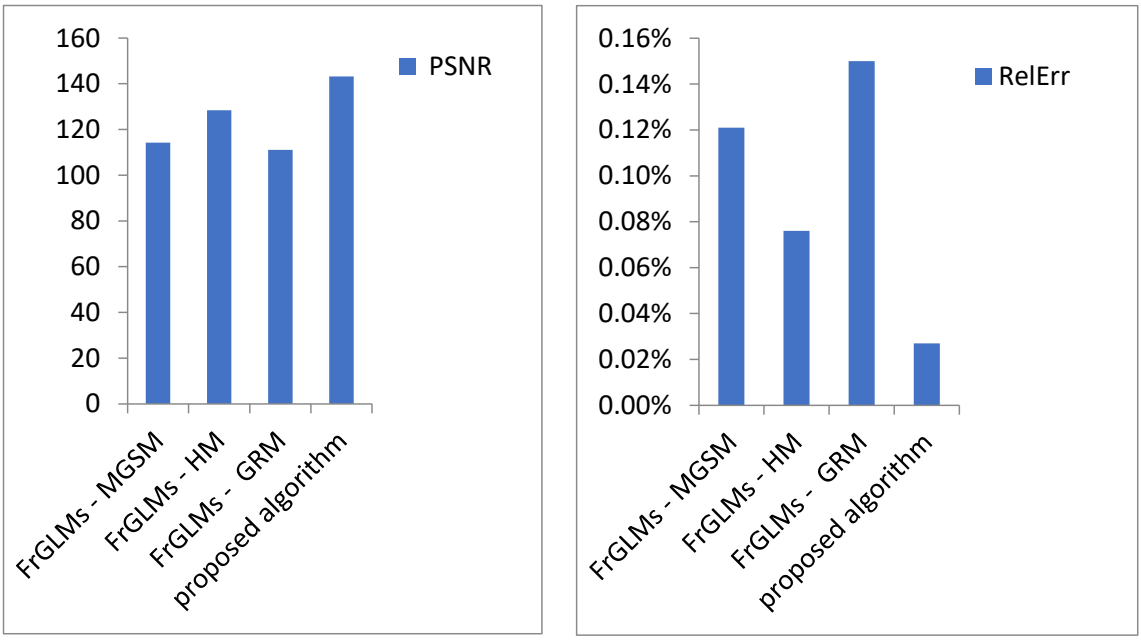


**Figure 3.** The average values of quality metrics (PSNR and RelErr (%)) for the introduced algorithm and FrGLMs—GSM, FrGLMs—HM, and FrGLMs—GRM.

**Table 2.** Comparative results of the introduced algorithm with FrGLMs—GSM, FrGLMs—HM, and FrGLMs—GRM.

| Signal | FrGLMs—GSM | | | FrGLMs—HM | | | FrGLMs—GRM | | | Proposed Algorithm | | |
|---|---|---|---|---|---|---|---|---|---|---|---|---|
| | PSNR | MSE | RelErr (%) | PSNR | MSE | RelErr (%) | PSNR | MSE | RelErr (%) | PSNR | MSE | RelErr (%) |
| **Rec. 101** | 109.60 | 0.0359 | 0.089 | 128.22 | 0.01743 | 0.043 | 111.91 | 0.02548 | 0.063 | 141.05 | 0.00992 | 0.025 |
| **Rec. 108** | 93.022 | 0.2066 | 0.512 | 108.39 | 0.1064 | 0.264 | 88.38 | 0.2723 | 0.675 | 119.92 | 0.01496 | 0.037 |
| **Rec. 115** | 124.20 | 0.0203 | 0.050 | 139.72 | 0.01358 | 0.034 | 118.55 | 0.029792 | 0.074 | 155.46 | 0.00328 | 0.008 |

**Table 2.** *Cont.*

| Signal | FrGLMs—GSM | | | FrGLMs—HM | | | FrGLMs—GRM | | | Proposed Algorithm | | |
|---|---|---|---|---|---|---|---|---|---|---|---|---|
| | PSNR | MSE | RelErr (%) | PSNR | MSE | RelErr (%) | PSNR | MSE | RelErr (%) | PSNR | MSE | RelErr (%) |
| **Rec. 209** | 109.06 | 0.0210 | 0.052 | 120.78 | 0.01967 | 0.049 | 104.73 | 0.029792 | 0.074 | 135.82 | 0.00728 | 0.018 |
| **Rec. 214** | 112.64 | 0.0508 | 0.126 | 124.86 | 0.04214 | 0.104 | 109.09 | 0.05985 | 0.148 | 139.80 | 0.0304 | 0.075 |
| **Rec. 219** | 129.54 | 0.0195 | 0.048 | 144.22 | 0.01491 | 0.037 | 128.10 | 0.02044 | 0.051 | 163.20 | 0.0080 | 0.020 |
| **Rec. 230** | 123.72 | 0.0142 | 0.035 | 135.56 | 0.01351 | 0.033 | 120.46 | 0.01631 | 0.040 | 151.41 | 0.00456 | 0.011 |
| **Rec. 234** | 112.09 | 0.0219 | 0.054 | 125.26 | 0.01652 | 0.041 | 107.287 | 0.02947 | 0.073 | 139.05 | 0.00936 | 0.023 |
| **Average** | **114.23** | **0.0487** | **0.121** | **128.37** | **0.03052** | **0.076** | **111.06** | **0.06041** | **0.150** | **143.21** | **0.01096** | **0.027** |

To confirm the superiority of the proposed algorithm in reconstruction quality, Figure 3 presents a set of reconstructed "Rec. 101" signal in terms of PSNR and RelErr for the introduced algorithm and FrGLMs—GSM, FrGLMs—HM, and FrGLMs—GRM. The results in Table 2 and Figures 3 and 4 demonstrate that the proposed algorithm has the best PSNR, MSE, and RelErr corresponding to all the used signals and the total average of PSNR, MSE, and RelErr.

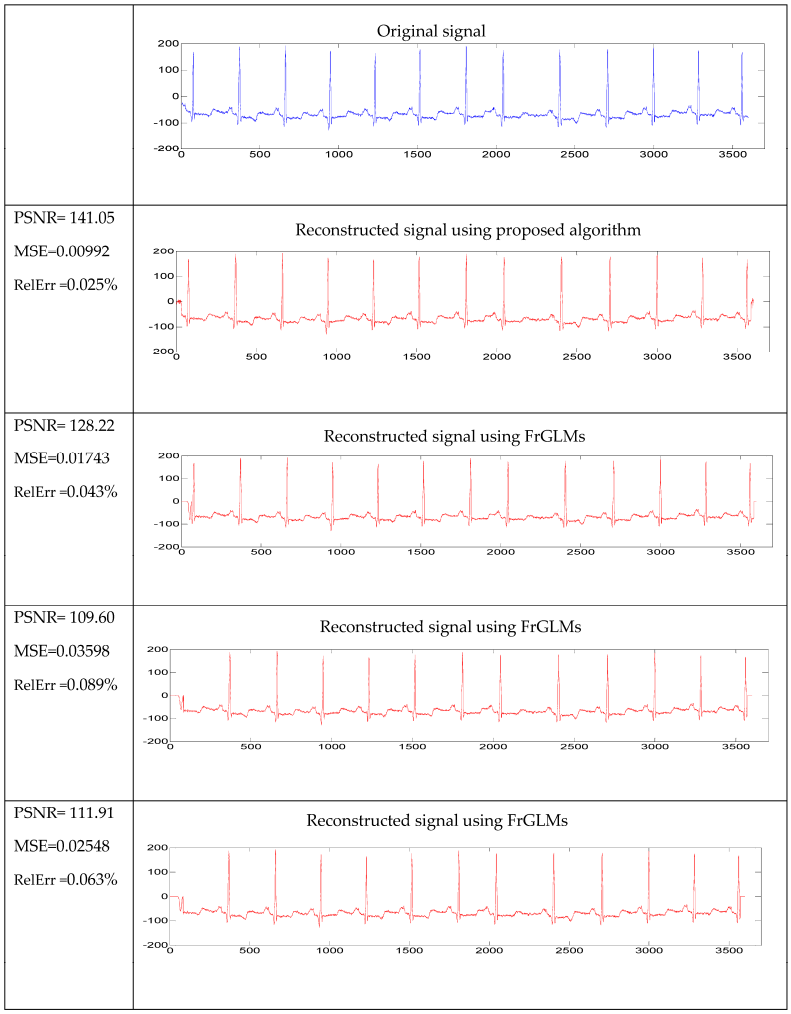


**Figure 4.** Set of reconstructed "Rec. 101" signal employing the introduced algorithm and FrGLMs—GSM, FrGLMs—HM, and FrGLMs—GRM.

A comparison is conducted between the proposed algorithm and FrGLMs—HM in reconstruction with orders from 50 and 500 to make the results more accurate. Table 3 presents the comparative results of the proposed algorithm and FrGLMs—HM in PSNR, MSE, and RelErr (%). The PSNR and MSE curves for the reconstructed signals (Rec. 101 and Rec. 219) at various orders from 50 to 500 are shown in Figures 5 and 6, respectively. As shown in Table 3 and Figure 5, the PSNR values increase proportionally as the number of moment orders increases, indicating an enhancement in the reconstructed signal quality. As shown in Table 3 and Figure 6, the best value of MSE is likewise obtained as the number of moment orders increases. The results also outperform the introduced algorithm compared to FrGLMs—HM at each order in terms of PSNR and MSE.

**Table 3.** Performance of introduced algorithm compared to FrGLMs—HM in various orders.

| Signal | Order | FrGLMs—HM | | Proposed Algorithm | |
|---|---|---|---|---|---|
| | | PSNR | MSE | PSNR | MSE |
| **Rec. 101** | 50 | 85.104 | 0.8541 | 88.104 | 0.3479 |
| | 100 | 90.658 | 0.3140 | 93.487 | 0.2011 |
| | 200 | 110.847 | 0.0220 | 119.639 | 0.0194 |
| | 300 | 116.014 | 0.0200 | 132.541 | 0.0148 |
| | 400 | 121.583 | 0.1984 | 137.965 | 0.0117 |
| | 500 | 128.22 | 0.01743 | 141.05 | 0.0099 |
| **Rec. 219** | 50 | 89.417 | 0.3851 | 105.487 | 0.1961 |
| | 100 | 101.541 | 0.2604 | 116.541 | 0.1358 |
| | 200 | 114.981 | 0.0833 | 129.574 | 0.0504 |
| | 300 | 125.635 | 0.0293 | 145.654 | 0.0117 |
| | 400 | 136.992 | 0.0199 | 157.541 | 0.0098 |
| | 500 | 144.22 | 0.0149 | 163.20 | 0.0080 |

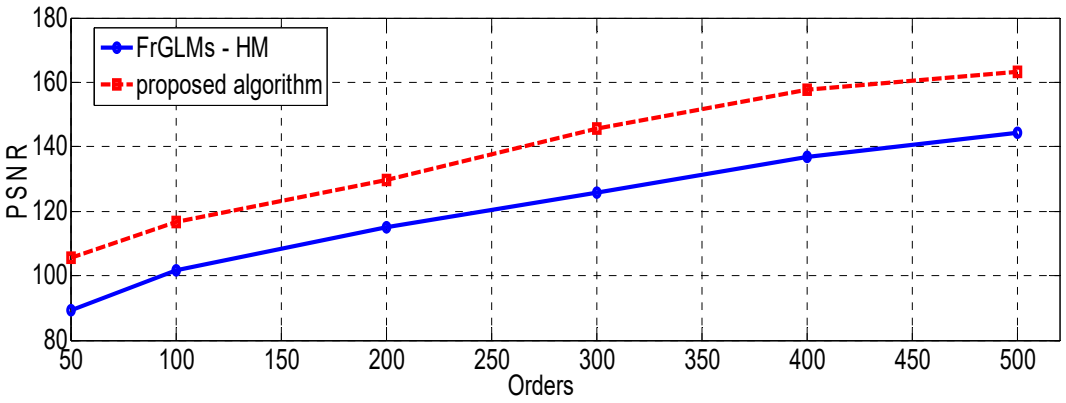


**Figure 5.** Values of PSNR for the reconstructed signal "Rec. 219" based on the proposed algorithm and FrGLMs—HM at different orders.

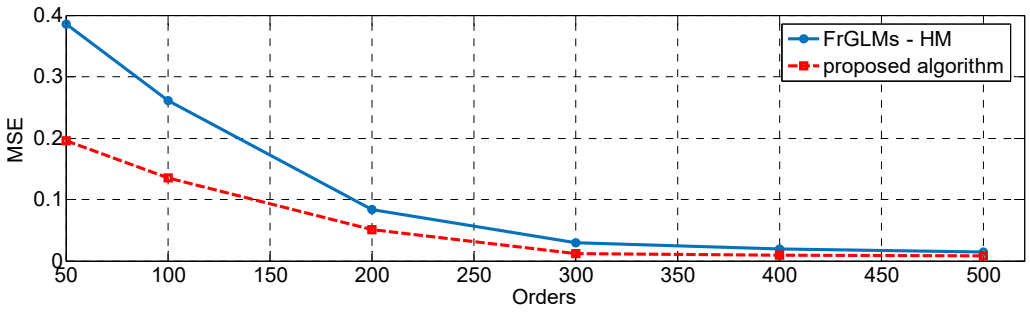


**Figure 6.** Values of MSE for the reconstructed signal "Rec. 219" based on the proposed algorithm and FrGLMs—HM at different orders.

A comparative investigation of other existing algorithms [8,18,20,36] in reconstruction quality is summarized in Table 4. Figures 7 and 8 display a graphic comparison of the introduced algorithm and other existing algorithms concerning PSNR and MSE, respectively. As shown in Table 4 and Figures 7 and 8, the proposed algorithm outperforms the existing algorithms, which have very high PSNR and the lowest MSE values.

**Table 4.** Comparative results of the introduced algorithm with other existing algorithms.

| Techniques | MSE | PSNR |
|---|---|---|
| **Charlier Moment—GSOP [8]** | 0.883 | 95.741 |
| **Krawtchouk—Householder [18]** | 0.0771 | 105.015 |
| **Meixner- MGS [20]** | 0.0948 | 85.654 |
| **Tchebichef–Householder [18]** | 0.0436 | 107.085 |
| **Hahn Moment Invariants (HMIs) [36]** | 0.0805 | 97.548 |
| **Proposed algorithm** | 0.0109 | 143.21 |

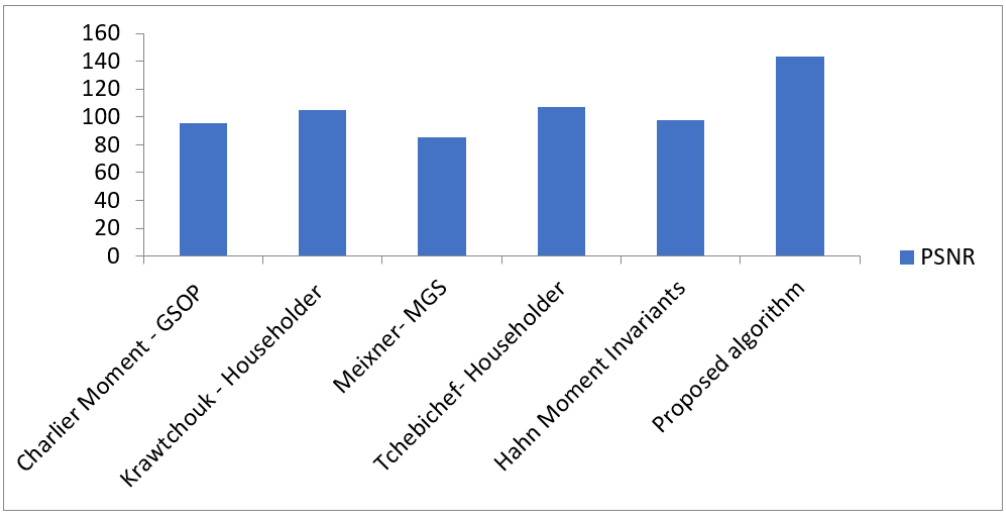


**Figure 7.** The average values of PSNR for the introduced algorithm compared with other existing algorithms.

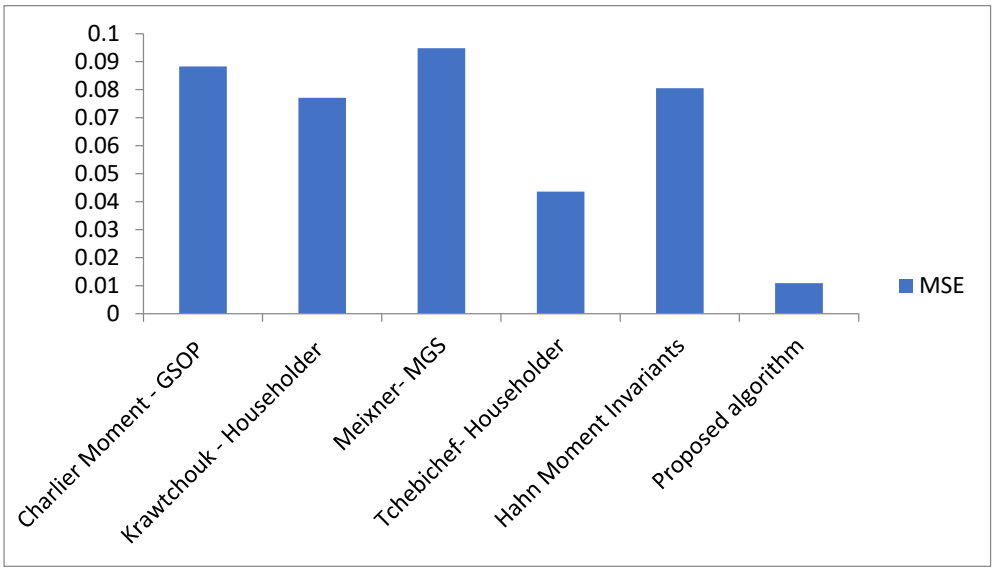


**Figure 8.** The average values of MSE for the introduced algorithm compared with other existing algorithms.

A comparative analysis is performed between the proposed algorithm and other existing algorithms in the context of reconstruction to ensure the accuracy of the proposed method. The analysis includes orders ranging from 50 to 500. Table 5 illustrates the comparison outcomes of the introduced and existing algorithms in terms of PSNR and MSE. Figures 9 and 10 display the PSNR and MSE curves corresponding to the reconstructed signal "Rec. 101" over different orders ranging from 50 to 500. The obtained results demonstrate the superior performance of the proposed method over the existing algorithms at every order, determined by PSNR and MSE.

**Table 5.** Performance of introduced algorithm compared to other existing algorithms in various orders.

| Signal | Order | Tchebichef–Householder [18] | | Krawtchouk—Householder [18] | | Proposed Algorithm | |
|---|---|---|---|---|---|---|---|
| | | PSNR | MSE | PSNR | MSE | PSNR | MSE |
| Rec. 101 | 50 | 75.232 | 0.949 | 73.048 | 1.2201 | 88.104 | 0.3479 |
| | 100 | 80.335 | 0.5273 | 77.213 | 0.7554 | 93.487 | 0.2011 |
| | 200 | 106.854 | 0.0249 | 104.067 | 0.0343 | 119.639 | 0.0194 |
| | 300 | 122.548 | 0.0201 | 118.474 | 0.03 | 132.541 | 0.0148 |
| | 400 | 129.198 | 0.0197 | 125.985 | 0.0284 | 137.965 | 0.0117 |
| | 500 | 132.017 | 0.0158 | 128.811 | 0.0203 | 141.05 | 0.0099 |

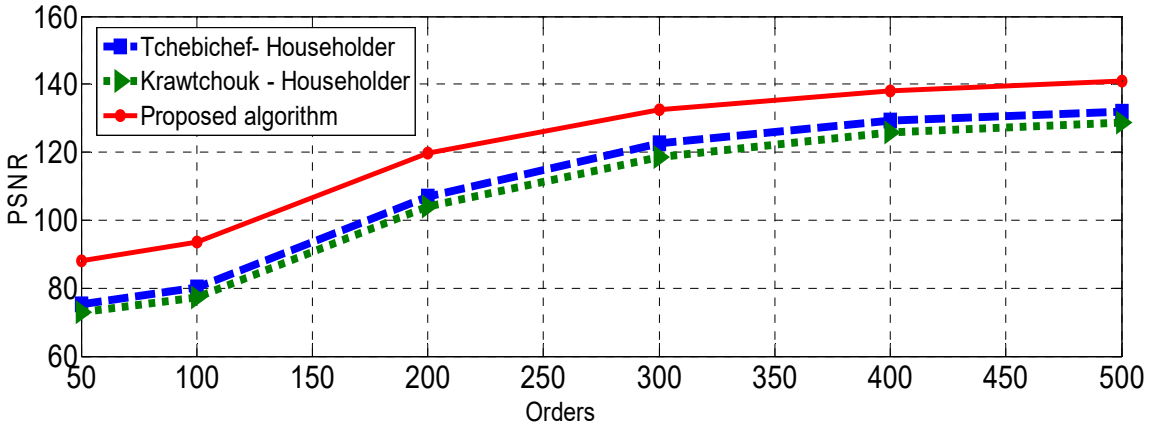


**Figure 9.** Values of PSNR of the reconstructed signal "Rec. 101" for the proposed algorithm and other existing algorithms at different orders.

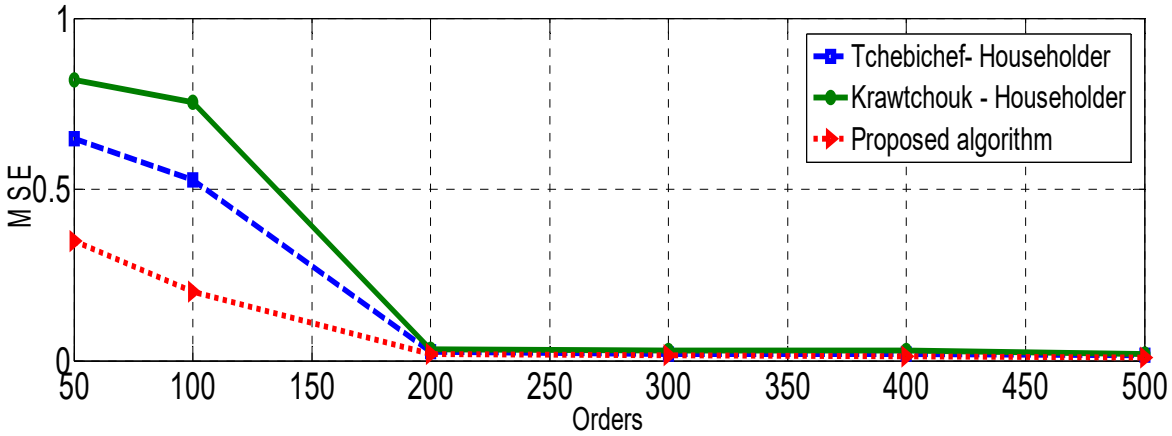


**Figure 10.** Values of MSE of the reconstructed signal "Rec. 101" for the proposed algorithm and other existing algorithms at different orders.

To investigate the complexity of the introduced algorithm, we compare the elapsed reconstruction time of the proposed algorithm and FrGLMs—GSM, FrGLMs—HM, and

FrGLMs—GRM. As shown in Figure 11, the proposed algorithm outperforms other algorithms in the elapsed reconstruction time at different orders. The visual inspection in Figure 11 shows that the introduced algorithm has less reconstruction time than FrGLMs—HM, FrGLMs—GRM, and FrGLMs—GSM. Table 6 and Figure 12 compare the introduced algorithm and the FrGLMs—HM algorithm in the elapsed reconstruction time and efficiency gain. The numerical results in Table 6 show that the elapsed reconstruction time of the proposed algorithm for the Rec. 101 signal is 0.7 s in contrast to 1.5 s for FrGLMs—HM. Also, concerning the Rec. 219 signal, the proposed algorithm elapses 0.9 s compared to 1.7 for FrGLMs—HM.

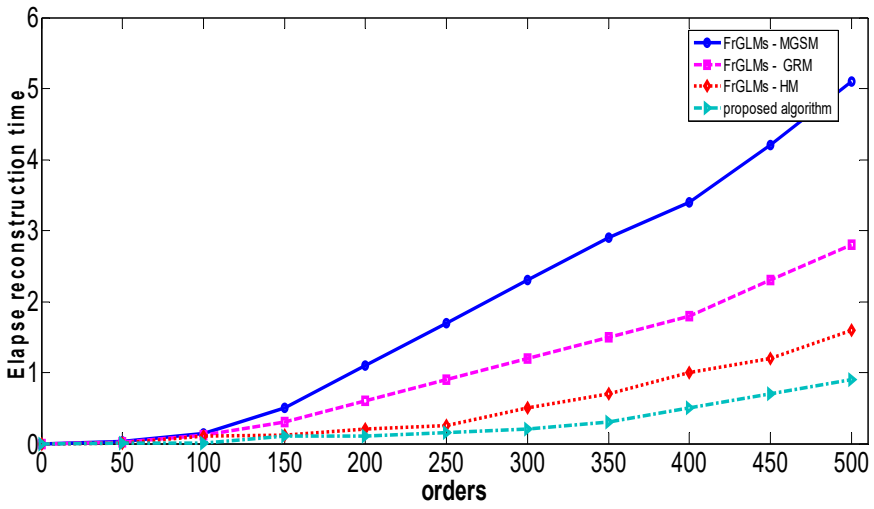


**Figure 11.** Elapsed reconstruction time for the proposed algorithm, FrGLMs—GSM, FrGLMs—HM, and FrGLMs—GRM at different orders.

**Table 6.** Elapsed reconstruction time of the proposed algorithm and FrGLMs—HM.

| | **Elapsed Reconstruction Time (s)** | |
|---|---|---|
| | **Rec. 101** | **Rec. 219** |
| **FrGLMs—HM** | 1.5 | 1.7 |
| **Proposed algorithm** | 0.7 | 0.9 |
| **Efficiency Gain** | **0.8** | **0.8** |

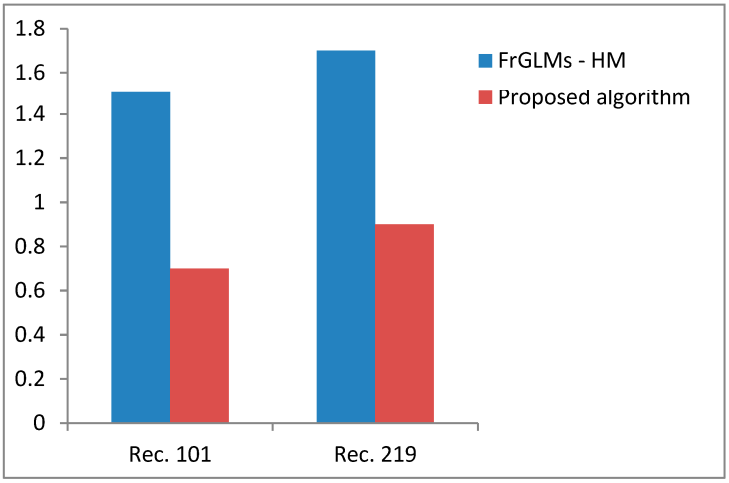


**Figure 12.** Comparison of elapsed reconstruction time between the proposed algorithm and FrGLMs—HM for "Rec. 101" and "Rec. 219" signals.

## 7. Discussion

This paper introduces a reconstruction algorithm based on FrGLMs and the Schwarz–Rutishauser algorithm. As seen previously and from the results of the comparative experiments, the proposed algorithm outperforms the algorithm that uses FrGLMs with GSM, HM, and GRM methods. The proposed algorithm was evaluated by assessing the quality of the reconstructed signal in terms of the elapsed time of reconstruction. The proposed method excelled in both aspects. The good results in quality reconstruction and elapsed reconstruction time go back to two main reasons. The first uses set fractional-order generalized Laguerre moments (FrGLMs), in which the term second-order recurrence formula is derived for the normalized form of the FrGLMs. Also, using the simple recursive formula of the gamma function, we deduced a recursive formula for evaluating the squared norm $h_k^{(\propto,\lambda)}$. It has great benefits in saving computation time. The second reason is using the Schwarz–Rutishauser algorithm to preserve the orthogonality property. The empirical experiments reveal that using the Schwarz–Rutishauser algorithm with FrGLMs takes less elapse time in reconstruction. In contrast to using the GSM, HM, and GRM methods with FrGLMs, due to its complexity, the Schwarz–Rutishauser algorithm is $(\boldsymbol{mn}^2)$, which is $(\boldsymbol{n})$-times less than GSM.

## 8. Conclusions

In conclusion, we would like to point out that we have provided an ideal approach for large-size bio-signals. The proposed approach is based on an ultramodern set of DOMs called FrGLMs. For more fast and accurate calculations, we derived a term second-order recurrence formula for the normalized form of FrGLMs. Also, we used a novel QR decomposition method called Schwarz–Rutishauser, which gives more accurate and stable calculations, especially at higher orders of FrGLMs. The MIT-BIH Arrhythmia Dataset analyzed the proposed algorithm's performance concerning MSE, PSNR, and elapsed reconstruction time. The empirical results reveal superiority in favor of the proposed algorithm (i.e., FrGLMs with the Schwarz–Rutishauser algorithm) when compared with FrGLMs with the classical QR decomposition techniques (i.e., GSM, HM, and GRM). Regarding the PSNR metric, the proposed algorithm gives average efficiency gain with values of 28.98, 14.84, and 32.15 when compared with FrGLMs—MGSM, FrGLMs—HM, and FrGLMs—GRM, respectively. The MSE metric gives average efficiency gain with values of 0.03784, 14.84, and 32.15 when compared with FrGLMs—MGSM, FrGLMs—HM, and FrGLMs—GRM, respectively. The proposed approach also achieves high superiority concerning the elapsed reconstruction time.

**Author Contributions:** Conceptualization, G.H., I.S.F. and K.M.H.; methodology, G.H., I.S.F. and K.M.H.; software, G.H., I.S.F. and K.M.H.; validation, G.H., I.S.F., K.M.H., D.S.K. and E.A.A.; formal analysis, G.H., I.S.F., K.M.H., D.S.K. and E.A.A.; investigation, D.S.K.; resources, D.S.K., E.A.A. and I.S.F.; data curation, G.H., I.S.F., D.S.K. and E.A.A.; writing—original draft preparation, G.H. and I.S.F.; writing—review and editing, K.M.H.; visualization, G.H., I.S.F., K.M.H., D.S.K. and E.A.A.; supervision, K.M.H.; project administration, D.S.K. and E.A.A.; funding acquisition, D.S.K. and E.A.A. All authors have read and agreed to the published version of the manuscript.

**Funding:** Princess Nourah bint Abdulrahman University Researchers Supporting Project number (PNURSP2023R409), Princess Nourah bint Abdulrahman University, Riyadh, Saudi Arabia.

**Data Availability Statement:** Data will be available open a responsible request.

**Conflicts of Interest:** The authors declare no conflict of interest to report regarding the present study.

## References

1. Flusser, J.; Suk, T.; Zitová, B. *Moments and Moment Invariants in Pattern Recognition*, 1st ed.; Wiley Online Library: London, UK, 2009; pp. 18–20.
2. Mukundan, R.; Ong, S.H.; Lee, P.A. Image analysis by Tchebichef moments. *IEEE Trans. Image Process.* **2001**, *10*, 1357–1364. [CrossRef] [PubMed]

3. Yap, P.T.; Paramesran, R.; Ong, S.H. Image analysis by Krawtchouk moments. *IEEE Trans. Image Process.* **2003**, *12*, 1367–1377. [PubMed]
4. Yap, P.T.; Paramesran, R.; Ong, S.H. Image analysis using Hahn moments. *IEEE Trans. Pattern Anal. Mach. Intell.* **2007**, *29*, 2057–2062. [CrossRef] [PubMed]
5. Zhu, H.; Shu, H.; Zhou, J.; Luo, L.; Coatrieux, J. Image analysis by discrete orthogonal dual Hahn moments. *Pattern Recognit. Lett.* **2007**, *28*, 1688–1704. [CrossRef]
6. Zhu, H.; Shu, H.; Liang, J.; Luo, L.; Coatrieux, J.-L. Image analysis by discrete orthogonal Racah moments. *Signal Process.* **2007**, *87*, 687–708. [CrossRef]
7. Xiao, B.; Luo, J.; Bi, X.; Li, W.; Chen, B. Fractional discrete Tchebyshev moments and their applications in image encryption and watermarking. *Inf. Sci.* **2020**, *516*, 545–559. [CrossRef]
8. Daoui, A.; Yamni, M.; Elogri, O.; Karmouni, H.; Sayyouri, M.; Qjidaa, H. Stable computation of higher order Charlier moments for signal and image reconstruction. *Inf. Sci.* **2020**, *521*, 251–276. [CrossRef]
9. Hassan, G.; Hosny, K.M.; Farouk, R.M.; Alzohairy, A.M. An efficient retrieval system for biomedical images based on radial associated Laguerre moments. *IEEE Access* **2020**, *8*, 175669–175687. [CrossRef]
10. Wu, H.; Yan, S. Computing invariants of Tchebichef moments for shape based image retrieval. *Neurocomputing* **2016**, *215*, 110–117. [CrossRef]
11. Ernawan, F.; Kabir, N.; Zamli, K.Z. An efficient image compression technique using Tchebichef bit allocation. *Optik* **2017**, *148*, 106–119. [CrossRef]
12. Xiao, B.; Lu, G.; Zhang, Y.; Li, W.; Wang, G. Lossless image compression based on integer Discrete Tchebichef Transform. *Neurocomputing* **2016**, *214*, 587–593. [CrossRef]
13. Liao, X.; Yu, Y.; Li, B.; Li, Z.; Qin, Z. A New Payload Partition Strategy in Color Image Steganography. *IEEE Trans. Circuits Syst. Video Technol.* **2019**, *30*, 685–696. [CrossRef]
14. Hosny, K.M.; Darwish, M.M. New geometrically invariant multiple zero-watermarking algorithm for color medical images. *Biomed. Signal Process. Control* **2021**, *70*, 103007. [CrossRef]
15. Hosny, K.M.; Khalid, A.M.; Mohamed, E.R. Efficient compression of bio-signals by using Tchebichef moments and Artificial Bee Colony. *Biocybern. Biomed. Eng.* **2018**, *38*, 385–398. [CrossRef]
16. Fathi, I.S.; Makhlouf, M.A.A.; Osman, E.; Ahmed, M.A. An Energy-Efficient Compression Algorithm of ECG Signals in Remote Healthcare Monitoring Systems. *IEEE Access* **2022**, *10*, 39129–39144. [CrossRef]
17. Fathi, I.S.; Ahmed, M.A.; Makhlouf, M.A. An efficient compression technique for Foetal phonocardiogram signals in remote healthcare monitoring systems. *Multimed. Tools Appl.* **2023**, *82*, 19993–20014. [CrossRef]
18. Fathi, I.S.; Ahmed, M.A.; Makhlouf, M.A. An efficient computation of discrete orthogonal moments for bio-signals reconstruction. *EURASIP J. Adv. Signal Process.* **2021**, *2022*, 107854. [CrossRef]
19. Daoui, A.; Yamni, M.; Karmouni, H.; El Ogri, O.; Sayyouri, M.; Qjidaa, H. Efficient Reconstruction and Compression of Large Size ECG Signal by Tchebichef Moments. In Proceedings of the 2020 International Conference on Intelligent Systems and Computer Vision (ISCV), Fez, Morocco, 9–11 June 2020.
20. Daoui, A.; Sayyouri, M.; Qjidaa, H. Efficient computation of high-order Meixner moments for large-size signals and images analysis. *Multimed. Tools Appl.* **2021**, *80*, 1641–1670. [CrossRef]
21. Mahmmod, B.M.; bin Ramli, A.R.; Abdulhussain, S.H.; Jassim, W.A.; Al-Haddad, S.A.R. Signal compression and enhancement using a new orthogonal-polynomial-based discrete transform. *IET Signal Process.* **2018**, *12*, 129–142. [CrossRef]
22. Kumar, A.; Ranganatham, R.; Singh, S.; Komaragiri, R.; Kumar, M. A robust digital ECG signal watermarking and compression using biorthogonal wavelet transform. *Res. Biomed. Eng.* **2021**, *37*, 79–85. [CrossRef]
23. Khaldi, A.; Kafi, M.R.; Meghni, B. Electrocardiogram signal security by digital watermarking. *J. Ambient. Intell. Humaniz. Comput.* **2022**, *14*, 13901–13913. [CrossRef]
24. Honarvar, B.; Paramesran, R.; Lim, C.-L. Image reconstruction from a complete set of geometric and complex moments. *Signal Process.* **2014**, *98*, 224–232. [CrossRef]
25. Imakura, A.; Morikuni, K.; Takayasu, A. Complex moment-based methods for differential eigenvalue problems. *Numer. Algorithms* **2023**, *92*, 693–721. [CrossRef]
26. Hosny, K.M.; Darwish, M.M.; Eltoukhy, M.M. Novel Multi-Channel Fractional-Order Radial Harmonic Fourier Moments for Color Image Analysis. *IEEE Access* **2020**, *8*, 40732–40743. [CrossRef]
27. Hosny, K.M.; Darwish, M.M.; Aboelenen, T. Novel fractional-order generic Jacobi-Fourier moments for image analysis. *Signal Process.* **2020**, *172*, 107545. [CrossRef]
28. Yamni, M.; Daoui, A.; El Ogri, O.; Karmouni, H.; Sayyouri, M.; Qjidaa, H.; Flusser, J. Fractional Charlier moments for image reconstruction and image watermarking. *Signal Process.* **2020**, *171*, 107509. [CrossRef]
29. Daoui, A.; Yamni, M.; Karmouni, H.; Sayyouri, M.; Qjidaa, H. Biomedical signals reconstruction and zero-watermarking using separable fractional order Charlier–Krawtchouk transformation and Sine Cosine Algorithm. *Signal Process.* **2020**, *180*, 107854. [CrossRef]
30. Gander, W. Algorithms for the QR decomposition. *Res. Rep.* **1980**, *80*, 1251–1268.

31. Bhrawy, A.H.; Alhamed, Y.A.; Baleanu, D.; Al-Zahrani, A.A. New spectral techniques for systems of fractional differential equations using fractional-order generalized Laguerre orthogonal functions. *Fract. Calc. Appl. Anal.* **2014**, *17*, 1137–1157. [CrossRef]
32. Meyer-Baese, U.; Muddu, H.; Schinhaerl, S.; Kumm, M.; Zipf, P. Real-Time Fetal ECG System Design Using Embedded Microprocessors. *SPIE Commer.+Sci. Sens. Imaging* **2016**, *9871*, 43–56. [CrossRef]
33. Giraud, L.; Langou, J.; Rozložník, M.; Eshof, J.V.D. Rounding error analysis of the classical Gram-Schmidt orthogonalization process. *Numer. Math.* **2005**, *101*, 87–100. [CrossRef]
34. Kroonenberg, P.M.; Ten Berge, J.M.F.; Brouwer, P.; Kiers, H.A.L. Gram-Schmidt versus Bauer-Rutishauser in alternating least-squares algorithms for three-mode principal component analysis. *Comput. Stat. Q.* **1989**, *5*, 81–87.
35. Shanthini, C. Matrix theory on QR decomposition. *Malaya J. Mat.* **2020**, *9*, 4127–4130.
36. Daoui, A.; Karmouni, H.; Sayyouri, M.; Qjidaa, H. Fast and stable computation of higher-order Hahn polynomials and Hahn moment invariants for signal and image analysis. *Multimed. Tools Appl.* **2021**, *80*, 32947–32973. [CrossRef] [PubMed]